Biomechanics of the Canine Mandible During Bone Transport Distraction Osteogenesis

5 authors, including:

Uriel Zapata
Universidad EAFIT
29 PUBLICATIONS **238** CITATIONS

SEE PROFILE

Paul C Dechow
Texas A&M University Baylor College of Dentistry
205 PUBLICATIONS **6,805** CITATIONS

SEE PROFILE

Mohammed Elsalanty
Augusta University
104 PUBLICATIONS **1,399** CITATIONS

SEE PROFILE

Lynne A Opperman
Texas A&M University College of Dentistry
181 PUBLICATIONS **5,301** CITATIONS

SEE PROFILE

Some of the authors of this publication are also working on these related projects:

Project — Evaluation of bone graft substitutes for the reconstruction of the alveolar cleft palate defect. View project

Project — Cranial Suture Functional Morphology View project

Uriel Zapata[1]
Mechanical Engineering Department,
EAFIT University,
Medellin 050022, Colombia
e-mail: uzapata@eafit.edu.co

Paul C. Dechow
Baylor College of Dentistry,
Texas A&M University,
Dallas, TX 75246
e-mail: pdechow@bcd.tamhsc.edu

Ikuya Watanabe
Department of Dental and Biomedical
Materials Science,
Nagasaki University Graduate School of
Biomedical Science,
Nagasaki 852-8523, Japan
e-mail: ikuyaw@nagasaki-u.ac.jp

Mohammed E. Elsalanty[1]
Department of Oral Biology and
Maxillofacial Surgery,
College of Dental Medicine,
Georgia Regents University,
Augusta, GA 30912
e-mail: melsalanty@gru.edu

Lynne A. Opperman
Baylor College of Dentistry,
Texas A&M University,
Dallas, TX 75246
e-mail: lopperman@bcd.tamhsc.edu

Biomechanics of the Canine Mandible During Bone Transport Distraction Osteogenesis

This study compared biomechanical patterns between finite element models (FEMs) and a fresh dog mandible tested under molar and incisal physiological loads in order to clarify the effect of the bone transport distraction osteogenesis (BTDO) surgical process. Three FEMs of dog mandibles were built in order to evaluate the effects of BTDO. The first model evaluated the mandibular response under two physiological loads resembling bite processes. In the second model, a 5.0 cm bone defect was bridged with a bone transport reconstruction plate (BTRP). In the third model, new regenerated bony tissue was incorporated within the defect to mimic the surgical process without the presence of the device. Complementarily, a mandible of a male American foxhound dog was mechanically tested in the laboratory both in the presence and absence of a BTRP, and mechanical responses were measured by attaching rosettes to the bone surface of the mandible to validate the FEM predictions. The relationship between real and predicted values indicates that the stress patterns calculated using FEM are a valid predictor of the biomechanics of the BTDO procedures. The present study provides an interesting correlation between the stiffness of the device and the biomechanical response of the mandible affected for bone transport. [DOI: 10.1115/1.4028409]

Introduction

Distraction osteogenesis is a surgical technique in which underdeveloped bones can be sectioned by corticotomy and then lengthened or widened by traction forces to correct bone growth deficiencies. The concept of lengthening bone by distraction forces was first described by an Italian doctor in 1905 [1]. By using distraction forces, Codivilla attempted to lengthen femurs and their related soft tissue in deformity cases in which the lower limbs were shortened. In 1927, Abbott from the Shriner's Hospital in St Louis, MO, presented an improved distraction device that was applied directly to the tibia to correct limb length discrepancies [2]. Early attempts to distract endochondral bones resulted in several clinical complications, such as skin necrosis, edema, infections, angular deviation, and delayed ossification of the lengthened segment [3].

As a result, the lengthening of human limbs by distraction techniques was temporarily discontinued. In its place, either an external prostheses to compensate the limb length difference or shortening the unaffected limb was used [4]. The endochondral bone distraction technique was abandoned until 1958 when Illizarov began his work on the surgical process of bone lengthening [5,6]. He diminished the previous clinical complications by performing a corticotomy, rather than an osteotomy, with minimal interruption of the periosteum, thus keeping blood supply to the bone tissues [3,4].

Distraction osteogenesis was first applied to the membranous bones of the craniofacial skeleton by Snyder et al. in 1973. They removed surgically a unilateral segment of bone (15 mm length) from dog mandibles, generating a severe crossbite that was then reopened using an external distraction device [7]. The mandibular distraction procedure was further developed by Michieli and Miotti in 1977. They performed bilateral distraction osteogenesis in two dogs using an external device to lengthen 15 mm of the mandible. Based on their results, they suggested the first mandibular distraction operative protocol in humans, involving a latency period of 1 week, an activation rate of 1 mm on alternate days, and a minimum consolidation period of 45 days for every 15 mm of distraction [8]. Later, Karp et al. [4], performed mandibular unilateral distraction osteogenesis procedure (20 mm length) on six mongrel dogs by using an external device similar to the one used by Snyder et al. [7]. They reported progressive calcification of the expanded segment, including vascular channels comparable to the native side [4]. Almost at the same time, the first mandibular BTDO procedure was performed in six mongrel dogs, divided into experimental and control groups, by Costantino et al. [9]. They reported good mandibular BTDO outcomes by preserving the soft tissue attached to the periosteal transport disk [9]. Later, in 1992, the first clinical distraction osteogenesis procedure was performed on the human mandible by McCarthy et al. [3], using an extra-oral distraction device [10]. They applied monofocal distraction techniques to four children with mandibular hypoplasia using either unilateral or bilateral treatments. Thenceforth, BTDO has been extensively used to reconstruct segmental mandibular defects by regenerating cortical bone [10–12].

Although the clinical use of BTDO has become one of the most feasible treatment options for the correction of mandibular deformities, the development of novel mandibular distraction devices requires experimentation on animals before their clinical use on human patients [13,14]. The dog distraction model has been the most widely used to study mandibular distraction

because the size of the mandibular structure allows not only the use of a similar distraction device, but also because mandibular bone resections can be recreated in analogous sizes to those seen in human patients [15]. Nevertheless, animal experimentation has two main disadvantages: first, regulations of the ethical treatment of animals tend to minimize their use; and secondly, results from animal models are difficult to extrapolate to humans because of the anatomical and functional differences [16]. A combination of both physical animal models (in vitro experiments) and computational models (FEM) may reduce the need for animal experimentation and increase the accuracy of the biomechanical results by using a validation process of the results. Additionally, FEM can be used as a tool to predict the biomechanical effects of the bone transport process in animal models before its application on human patients. The purpose of this work was to evaluate and validate the biomechanical patterns produced within the dog mandible in response to the complete BTDO surgical process with an internal bone transport device by testing and comparing a 3D FEM of the dog mandible with an in vitro test of the mandibular bone transport process.

Materials and Methods

Experimental Model. A freshly sacrificed and skeletally mature male beagle dog (12 months old) was used in this research design to test and validate bone transport effects [11,17]. The housing, care, and experimental protocols were in compliance with the Texas A&M University, Baylor College of Dentistry, Institutional Animal Care and Use Committee. Protocols allow for suitable conditions of lodging, health and feeding of animals, with facilities adapted for easy manipulation of the animal and the design of a balanced diet, which guarantees good nutrition. All procedures that caused pain in the animal were done with sedation, analgesic, or anesthetic and conformed to the accepted veterinary practices and norms for biomedical investigations with animals [18]. After the dog was sacrificed, for a research project unrelated with the present investigation, the skull was removed and a cone beam computed tomography scanner was used to record the radiographic information of all the tissues (i-CAD, IDT Dental Products Ltd, London, UK). The mandible was then dissected free from soft tissues and stored at $-20\,^\circ$C before lab testing.

All the surfaces of the mandible were degreased with n-propyl bromide and the surfaces to be used to glue the rosettes were sanded with 320 grit emery, wet sanded with 400 grit sand paper, and subsequently cleaned with a mild phosphoric acid compound and water-based ammonia cleaner (Micro-Measurements Division, Measurements Group, Inc., Raleigh, NC). Cortical bone strain data were recorded from five rectangular stacked rosette strain gauges (C2A-06-031WW-350, Micro-Measurements) placed on the lateral aspect of the dog mandible corpus and symphysis using M-Bond 200 adhesive. Because strain gauge location may affect strain reading reliability, the gage rosettes were placed

close to the basal border of the mandibular corpus in order to obtain simultaneously both normal bending and torsion shear strains (Fig. 1(a)). All rosettes were aligned with the basal mandibular plane to later obtain maximum strain orientation results. The surfaces of the rosettes were covered with polyurethane coating to offer mechanical protection to the gauge and the ends of the wires during test procedures. The positioning of the strain rosettes was as follows: (1) left buccal surface of the mandibular corpus under the first molar; (2) left lingual surface of the mandibular corpus under the first molar; (3) left buccal surface of the mandibular body under the third premolar; (4) at the left mandibular symphysis under the canine tooth; and (5) right buccal surface of the mandibular corpus under the third premolar.

A special frame was designed for fastening the mandible. Both the mandibular condyles and angular processes were fixed using metallic clamps complemented with self-polymerizing acrylic resin (Fig. 1(a)). In addition, the erect elements of the frame were designed in such a way that allowed bidirectional movement of the frame–mandible complex to facilitate the vertical load positioning at the testing machine. In the first set of loads applied to the complete mandible (condition 1), strain measurements were recorded from the stacked rosettes during simulated 256 N load applied on the first molar [19] and 100 N load applied to the first-incisors at a rate of 1 mm/min using a universal testing machine (Dual Column model 5860 series, Instron Co., Norwood, MA), which also recorded the vertical displacement at each of both load positions. In the second test (condition 2), a 5.0 cm segmental bone resection of the right molar region in the dog mandible was performed. A BTRP (Craniotech ACR Devices, LLC, Dallas, TX) was attached to the mandible by six cortical miniscrews resembling a bone transport surgical process [20] (Fig. 1(b)), and comparable strain gauge readings were performed. Although the fifth rosette was removed during this latest surgical procedure, the mandible was then tested with the same loads, at the same places as previously described, and consequently the strain patterns were measured in four rosette gauges attached to the left side of the mandible.

All the rosettes were connected to a series of sensor interface hardware amplifiers (PCD-300 A, Kyowa Electronic Instruments Co., Ltd, Japan) to record changes in electrical resistance during the application of simulated bite forces on the mandible. The electrical resistance changes were converted from analog to digital data and from there into strain values by using control software (Kyowa PCD-30 A, Ver.01.07, Soltec co, San Fernando, CA). Normal strain, defined as $\varepsilon_i = dL/L$, was measured in every gauge component of the rosettes and their values processed to obtain both maximum (ε_{max}) and minimum (ε_{min}) normal strains at every selected point. Direction of principal strain orientation (θ) was calculated with respect to gauge number one, and maximum shear strain (γ_{max}) was derived by averaging the maximum and minimum normal strain values [21]. Strain is unit-less, and it is given in microstrains [$\mu\varepsilon = 1 \times 10^{-6}$].
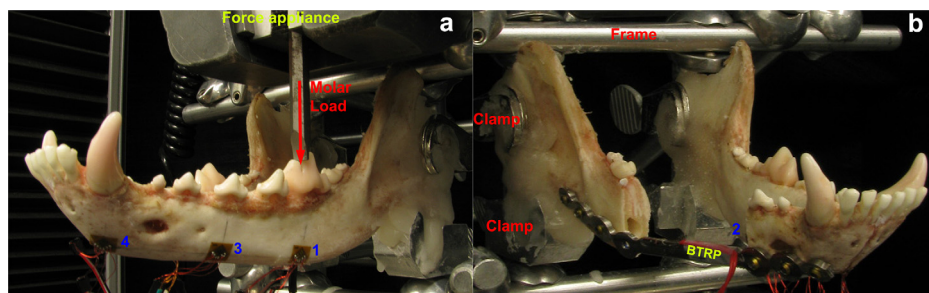

Fig. 1 In vitro models of the dog mandible placed on the frame. (a) Complete mandible tested in the laboratory under static vertical load on the left first molar to record the strains using rosettes. Rosettes 1, 3, and 4 are presented. (b) Canine mandible with the BTRP device bridging the created bone defect on the right side of the mandible.

FEMs. FEM is an engineering tool that is extensively used in mandibular bone biomechanics by subdividing the mandibular complex geometry into small simpler geometrical elements [16,22]. FEM allows creation of computational models by defining geometry, mechanical properties, loads, and boundary conditions. Finally, FEM generates results in terms of strains, stresses, and deformations at the nodes of the model by solving partial differential equations.

Morphological information from the fresh dog mandible (Fig. 2(a)), including cortical bone, trabecular bone, cartilage, and teeth, was recorded from the computed tomography scan (CT-scan) into a digital imaging and communications in medicine (DICOM) file. The DICOM file was used for the first geometric reconstruction using a three dimensional reconstruction software package (Fig. 2(b)) (Mimics 13.0, Materialise, Leuven, Belgium). Complementarily, a FEM module from the Mimics software was used for the first mesh definition of the mandible and associated structures [16]. The three-dimensional (3D) outer shapes were saved in a surface triangularized file format (STL) that were refined, cleaned, and smoothed in a reverse-engineering software (Geomagic studio-11, Geomagic Co, NC). Once more, the model was returned to Mimics software to obtain solid elements that were grouped into several volumes to assign different mechanical properties to the model. These 3D reconstructions were converted into full 3D FEM meshes (Fig. 2(c)) that were evaluated within an FEM software (Strand7, Strand7 Pty Ltd, Sydney, Australia). The mandibular FEM was composed of 200,743 brick elements in the cortical bone, 91,394 elements in the trabecular bone, 84,506 elements in the teeth, and 3456 elements in the cartilage tissue at the symphysis. Three different models of the dog mandible were considered under the effect of both 256 N molar and 100 N incisal bite forces in order to consider the three main stages of the mandibular BTDO process. First, the complete dog mandible was modeled in its original morphology without muscle effect (Fig. 3(a)), then the dog mandible model underwent a 5.0 cm bone resection to create a defect resembling the BTDO surgical excision and a BTRP device was modeled bridging the gap (Fig. 3(b)). Lastly, the dog mandible was modeled without the device, and including new bony tissue resembling that obtained after BTDO procedure (Fig. 3(c)).

Mechanical properties for the cortical bone, regenerated bone, trabecular bone, dentin, BTRP device, and symphysis were not only evaluated but also assumed from several authors[12,23–25] (Table 1). A previous study from the authors reported the mechanical properties of the regenerate dog cortical bone are not only heterogeneous, but also tend to be approximately transversely
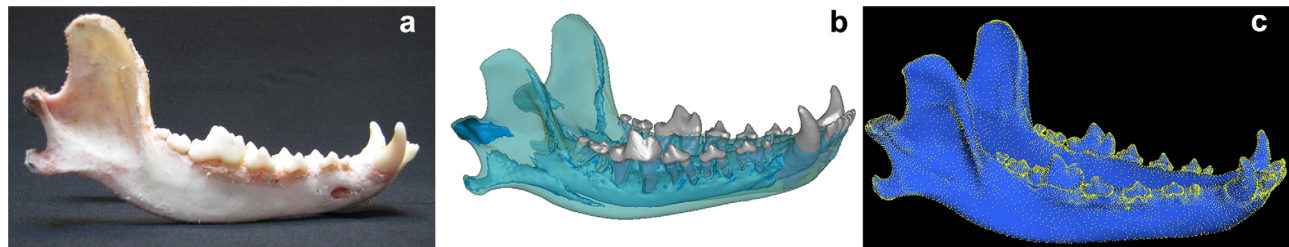

Fig. 2 Models of the dog mandible. (*a*) Fresh dissected mandible from the Beagle dog. (*b*) Computational 3D model of the mandible including teeth, cortical, and trabecular bone. (*c*) 3D-FEM of the mandible including its morphological structures.
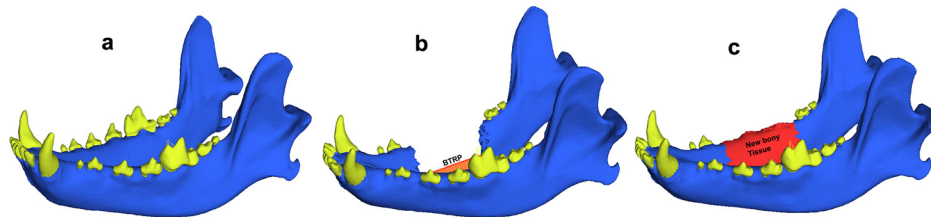

Fig. 3 3D-FEM of the dog mandible resembling the three medical conditions. (*a*) Complete mandible including cortical and trabecular bone, teeth, cartilage, and the symphysis. (*b*) 3D model of the resected mandible and the novel BTRP device bridging the defect (5 cm long). (*c*) 3D model of the reconstructed mandible including the new regenerated tissue. In the third case, the BTRP device was not included in order to simulate the postoperative process.

Table 1 Elastic mechanical properties of the materials used in the FEM of the distracted mandible including elastic moduli (E_1, E_2, E_3), Poisson's ratios (v_{12}, v_{13}, v_{23}), and shear moduli (G_{12}, G_{31}, G_{32}). Subscript values 1, 2, and 3 represent the three orthogonal principal directions.

Material	E_1 (GPa)	E_2 (GPa)	E_3 (GPa)	v_{12}	v_{13}	v_{23}	G_{12} (GPa)	G_{31} (GPa)	G_{32} (GPa)
Trabecular bone	10.5[a]	10.5[b]	10.5[b]	0.23[c]	0.23[c]	0.23[c]	—	—	—
Dentin	20.0[d]	20.0[d]	20.0[d]	0.32[d]	0.32[d]	0.32[d]	—	—	—
BTRP device[e]	114.0	114.0	114.0	0.34	0.34	0.34	—	—	—
Cortical Bone[f]	12.6	15.7	31.4	0.42	0.16	0.10	4.8	7.2	9.2
Regenerate bone[f]	9.9	11.7	23.1	0.45	0.20	0.08	3.7	5.6	7.0

[a]Modified to resemble isotropic behavior.
[b]Reference [25].
[c]Reference [24].
[d]Reference [23].
[e]Reference [29].
[f]Reference [26].

isotropic at a tissue level as opposed to control cortical bone that is orthotropic [26]. Isotropic elastic moduli of the dog trabecular bone were obtained from the ultrasonic test of the femora of eight dogs [25]. Poisson's Ratio in the trabecular bone was obtained from a 1 GHz acoustic microscope test [24]. The elastic properties for the dentin were obtained from a study that measured sound speed in bovine dentin and enamel [23]. Although mechanical properties of the symphysis can be modeled like those of cartilage of young adult Beagle dogs [27], their mechanical characteristics were assumed to be similar to trabecular bone to mimic the synostosis of the symphysis [28]. Finally, the BTRP device was assumed to be made from a titanium alloy Ti6Al4V (6% aluminum, 4% vanadium with extra interstitial elements, ELI), based on its biocompatibility characteristics, excellent corrosion resistance, fatigue properties, and its high strength–weight ratio [29].

The FEMs were calibrated and validated before interpretation. Calibration is a convergence test that measures the accuracy of the model by repeated refinement of the finite element mesh until the results are consistently similar. Calibration was performed, and the model is conformed for more than 31,7054 tetrahedral elements that guarantee the reliability of the results. Validation is an external process that assesses how accurately the computerized model represents the physical system by comparing FEM results with strain gauge results. The FEM was restricted from movement on both angular processes and mandibular condyles, resembling the same boundary conditions developed during lab tests, in order to guarantee the correlation between the strain results from the lab tests and the computational model [30]. Bite force was assumed to be 256 N for the molar position [19], and 100 N for the incisal position in order to compare the models in the lab with those from the computational simulations. Linear regression analysis was used to correlate the normal strains measured during the experimental tests with the normal strains predicted by the FEM at the same points.

Results

Experimental Model. Vertical deformations were measured at each point of load application with the universal testing machine. For instance, vertical deformation for the complete mandible under molar load was 1.21 for the complete mandible, and 1.15 mm for the distracted mandible. The vertical deformation under incisal load was 1.10 mm for the whole mandible, and 2.07 mm for the mandible including the BTRP device. The vertical displacements were similar for most of the biomechanical conditions, except when the device was bridging the mandible defect with the load applied on the incisors (Fig. 4).

Strain gauge data showed uniformly increasing strain patterns for all the rosette components. The maximum value is the greatest strain value in every gauge (ε_i). All the strains were reported in microstrain ($\mu\varepsilon$) which is equivalent to 1×10^{-6} strain. One of the components of rosette five did not work properly after several tests, so these data were not included in the second tests. In addition, the same rosette was removed during the surgical procedure, so the data were not recorded for the third and fourth experimental tests of the mandible. The greatest strain value (ε_i), recorded on every gauge for each load condition from the experimental tests, are presented in Table 2. By convention, tensile strains were represented as positive and compressive strains were represented as negative. Comparing strain results (ε_i) for the incisal position of the load, between the complete and the resected mandibles, the highest strain values were present in the resected mandible. The highest strain values (ε_i) are located in the posterior part of the mandible for the resected mandible; whereas they are located anteriorly for the complete mandible. Under molar loading, a similar distribution is found in the complete mandible; however, the distribution of the highest strains is reversed in the resected mandible.

Maximum principal strain (ε_{max}), minimum principal strain (ε_{min}), direction of maximum strain (θ), and maximum shear strain
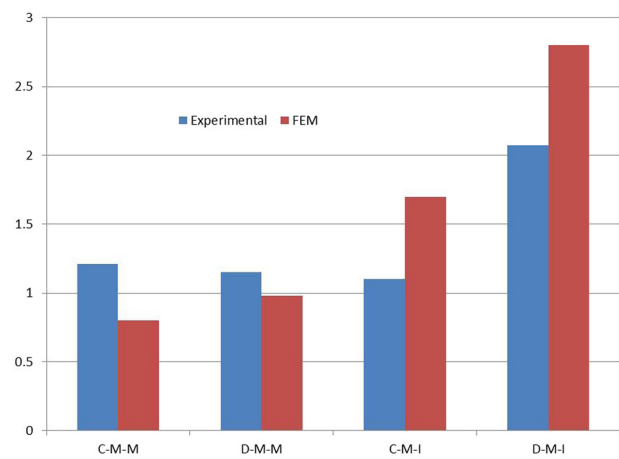

Fig. 4 Vertical displacement (mm) obtained from computational and experimental models at the places that the loads were applied. C-M-M (complete-mandible-molar load), D-M-M (distracted-mandible-molar load), C-M-I (complete-mandible-incisal load), and D-M-I (distracted-mandible-incisal load).

($\gamma_{max} = \varepsilon_{max} - \varepsilon_{min}$) were calculated from the extreme strains recorded at every gauge component by using Mohr's circle definition for principal strains [21]. In general, the maximum values of principal strains (ε_{max}, ε_{min}, γ_{max}) were present for the complete mandible under molar force, and oppositely, they were critical in the resected mandible under incisal load. Also, directions of maximum strain (θ), which indicate the direction of the maximum strains, were represented as positive if counterclockwise, or negative if clockwise. Angle variations among the four experimental tests are presented in Fig. 5. No differences were found, except for the posterior position of the resected mandible (Rosette 1) under the incisal load.

FEM. Vertical deformation and stress patterns are reported for the 100 N incisal load (Fig. 6), and for the 256 molar load (Fig. 7). The results, for both incisal and molar load conditions, are presented comparing the complete mandible, the resected mandible, and the mandible after the surgical procedure with the new, regenerated cortical bone (Figs. 6,7). The most critical biomechanical condition was present when the mandible has the defect bridged by the device, showing higher deformations patterns combined with changes in stress patterns for both load conditions.

The deformation patterns were symmetrical for the whole mandible during the incisal load condition (Fig. 6). However, the resected mandible presented twice the maximum vertical deformation (3.8 mm) compared to both the preoperative condition (1.9 mm) and the reconstructed mandible (2.0 mm). Deformation load patterns were similar for the three mandibular models under molar load condition (Fig. 7), but the vertical deformations were higher on the side that the load was applied to the mandible. The maximum vertical deformation was similar for both the preoperative condition (1.38 mm) and the reconstructed mandible (1.41 mm), however it was larger for the resected mandible wearing the BTRP device (2.20 mm), confirming biomechanical changes during the operative process of mandibular BTDO. Validation of the vertical deformation by comparing experimental displacements at the points where the loads were applied and the vertical displacements at the same points on the computational models showed slight similarities (Fig. 4). Molar displacements were 0.98 mm at the distracted mandible and 0.8 mm at the complete mandible. Complementarily, incisal displacements were 2.8 mm on the distracted mandible and 1.7 mm on the complete mandible (Fig. 4).

Stress patterns for the incisal load (Fig. 6) were not only similar but also symmetric for both the preoperative and the reconstructed

Table 2 Strain measurements recorded from each rosette gauge (ε_i), measured in microstrain units. Maximum (ε_{max}), and minimum normal strains (ε_{min}), measured in microstrain units, which were computed from the three measured strains. Maximum shear strain (γ_{max}), measured in microstrain units. Orientation of maximum strain referred to the first rosette gauge (θ), measured in degree units. Condition 1 is referred to the complete mandible, whereas condition 2 is associated with the resected mandible with the attached BTRP device.

Gauge	Molar condition 1					Incisal condition 1					Molar condition 2					Incisal condition 2				
	ε_i	θ	ε_{max}	ε_{min}	γ_{max}	ε_i	θ	ε_{max}	ε_{min}	γ_{max}	ε_i	θ	ε_{max}	ε_{min}	γ_{max}	ε_i	θ	ε_{max}	ε_{min}	γ_{max}
1-1	192.5	−6.2	197.0	−184.5	381.5	−17.5	−40.5	132.1	−222.1	354.3	170	−21.8	244.3	−296.8	541.1	−137.5	42.6	241.2	−458.7	699.9
1-2	47.5					130					160					240				
1-3	−180					−72.5					−222.5					−80				
2-1	45	40.7	207.2	−174.7	381.9	27.5	−33.8	104.4	−144.4	248.8	72.5	29.0	131.5	−119.0	250.4	−20	−40.9	174.8	−279.8	454.7
2-2	−172.5					95					−100					172.5				
2-3	−12.5					−67.5					−60					−85				
3-1	−17.5	−27.5	174.6	−69.6	244.1	20	−26.8	92.0	−262.0	354.0	−15	−45[a]	10.0	−40.0	50.0	−80	−36.2	174.5	−554.5	729.0
3-2	−47.5					57.5					10					157.5				
3-3	122.5					−190					−15					−300				
4-1	−145	−19.0	116.0	−176.0	292.1	295	5.8	300.3	−220.3	520.7	−5	9.2	2.7	−5.2	7.9	162.5	−14.2	189.4	−256.9	446.3
4-2	−120					−12.5					0					72.5				
4-3	85					−215					2.5					−230				
5-1	−47.5	−38.7	81.5	−249.0	330.5	—	—	—	—	—	—	—	—	—	—	—	—	—	—	—
5-2	77.5					—					—					—				
5-3	−120					—					—					—				

[a]If $\varepsilon_1 = \varepsilon_3$ and $\varepsilon_2 < \varepsilon_1$, then $\theta = -45$ deg.

mandible conditions. However, the stress patterns changed dramatically for the resected mandible on the side of the mandible that the device was applied. The stress patterns for the molar load were analogous for the three mandibular models (Fig. 7), providing evidence for the direct effect of the molar load on the side of the mandible to which it is applied.

Principal strains were read on the mandible at the same locations the rosettes were attached in the in vitro test. A regression was performed between the maximum strains measured on the experimental tests and the maximum strains predicted for the FEMs (Fig. 8). A good linear correlation ($R^2 = 0.82$) was found between both the measured and the predicted maximum strains in the mandible.

Discussion

Mandibular BTDO is an alternative method to bone flap surgery for the correction of mandibular resections due to cancer, accidents or gunshot. This surgical process has been widely used not only because it has been shown that the quality of the new cortical bone created during the BTDO procedure resembles the original bone [26,31,32], but also because it allows early implants placement induced by the functional recovery of the mandible [33,34]. The present article provides evidence for a couple of biomechanical benefits of the mandibular BTDO process. First, there were analogous deformation patterns at the end of the mandibular transport distraction osteogenesis procedure when compared with the preoperative stage of the mandible, suggesting a complete retrieval of its biomechanical function. Similar stress outlines between the un-operated mandible and the reconstructed stage after the BTDO process also confirm the comprehensive retrieval of the mandibular function after the surgical process. Second, the presence of the bone transport device across the gap produced from the resected bone preserves the biomechanical function of the mandible. For instance, incisal biting loads were able to produce similar displacements in the mandible whether intact or not. Conversely, the molar load leads to asymmetrical deformation patterns.

Although it has been declared that no computational model can be completely validate because the validation process cannot be focused on the whole computational model [35,36], we stated that the biomechanical outputs obtained from validated computational models can be used to simulate the biomechanical response of biological tissues which can be used to make clinically relevant recommendations with sufficient level of accuracy. However, the clinical incidence of the biomechanical results obtained from computational models should be correctly interpreted by an interdisciplinary team before its predictions can be considered to have any real clinical confidence [37]. The validated computational model of a canine mandible representing the biomechanical effect of a BTDO surgical procedure may have two main impacts: (1) the significance of the observed correlations between predicted and measured strains shows that the stress patterns obtained from the FEM are an accurate predictor of the biomechanical responses of the dog mandible affected by BTDO; (2) our experimental results can be used in the future by other authors as a way for indirect validation of computational models of canine mandibles under BTDO procedures [38].

We have successfully established a dog model for mandibular bone distraction osteogenesis, which has several advantages. The dog mandible can be resected similar to that of humans, and the size of the mandible resembles the mandible in humans, thus the mandible of the beagle dog was able to receive a similar-sized device to that to be used in humans. However, extrapolation of mandibular BTDO results to humans should be made carefully, since no animal model is fully analogous to humans.

Biomechanical validation of FEM of the mandible can be attempted on synthetic, dry and wet mandibles by using three different options: Strain gauges [39], double exposure holography [30], and laser speckle interferometry [40]. The strain gauge
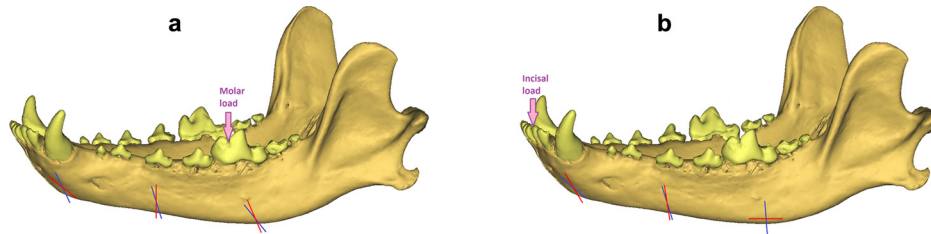
Fig. 5 Orientation of the principal strains obtained from the rosettes among the four experimental tests. The dashed line is associated with the complete model of the mandible (condition 1), whereas the solid line represents the presence of the BTRP device on the resected mandible (condition 2). (a) Molar force model and (b) incisor force model.
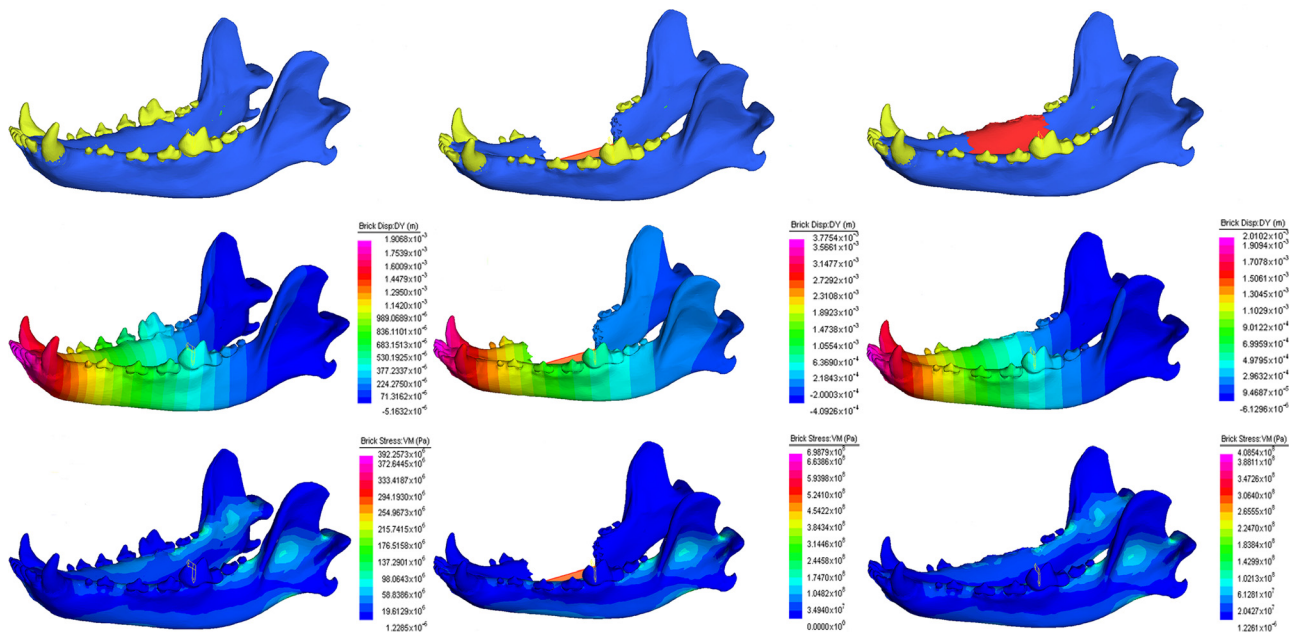

Fig. 6 Numerical results from the FEMs for the 100 N load applied at the incisal position. The first column represents the model of the mandible without surgical intervention; the second column represents the mandible at the earliest bone transport stage, including the device; and the third column represents the mandible with the newly formed bone tissue 12 weeks after distraction. The first row represents the vertical deformation patterns, and the second row shows the Von Misses stress patterns.

validation technique employed here has shown reliable results and has been used widely in bone biomechanics projects [41]. In this study, a fresh validated FEM has permitted predictions of the biomechanical response of the mandible affected by the surgical BTDO process.

The small differences in strains between the experimental test and the FEM could be due to practical difficulties attaching the strain gauges properly to the cortical bone surface, and critical electrical outcomes due to thermal effects during the recording process [42]. It is also important to consider the initial yield of the mandible and the support under the loading effect of the universal testing machine, and any possible slippage of the machine stick on the enamel of the tooth. It is also important to recognize the direct effect of the selected mechanical properties assigned to the model [41]. To our knowledge, no validated FEM has been done describing complete strain–stress patterns produced by the BTDO processes in the mandible.

Changes in stress patterns between the preoperative stage and the distracted mandible suggest an important biomechanical effect due to the presence of the BTDO device bridging the mandibular bone defect. The vertical deformations were similar for all the cases, except for the resected mandible loaded at the incisal position (Fig. 4). However, variability in the stress patterns trends suggests an indubitable change in the biomechanical conditions of the mandible due to the presence of the device, possibly due to the

fact that the device is stiffer than the surrounding bone, and it is applied to the inferior part of the mandibular body. Different strain values (ε_i) between gauges at rosettes 1 and 2, under incisal load suggest a complicated state of stresses within the mandible, which might include torsional effects, thus its biomechanical performance cannot be explained in terms of a simple cantilever beam.

This study presents several limitations. First, this project has a limited sample size involving only one dog mandible. However, this number was adequate to validate the multiple FEMs provided to test several biomechanical scenarios. In addition, although individual variations among biological parameters would affect conclusions, a validated FEM can represent accurately the irregular geometry and the lack the homogeneity of the mandible bone [43]. Second, the presence of masticatory muscles was not included within the models, thus the direct effect of them over the biomechanical response of the distracted mandible is unknown. Third, the mandibular condyles were completely restricted during the biomechanical evaluations. Although this simplification would affect any interaction with the maxilla, no significant biomechanical effects were expected within the mandibular body. Fourth, only one mandibular anatomical position of the distraction device was considered. Although many places could be considered for its placement, the device was specifically developed for straight bone transport at the body of the mandible, thus the ramus and the
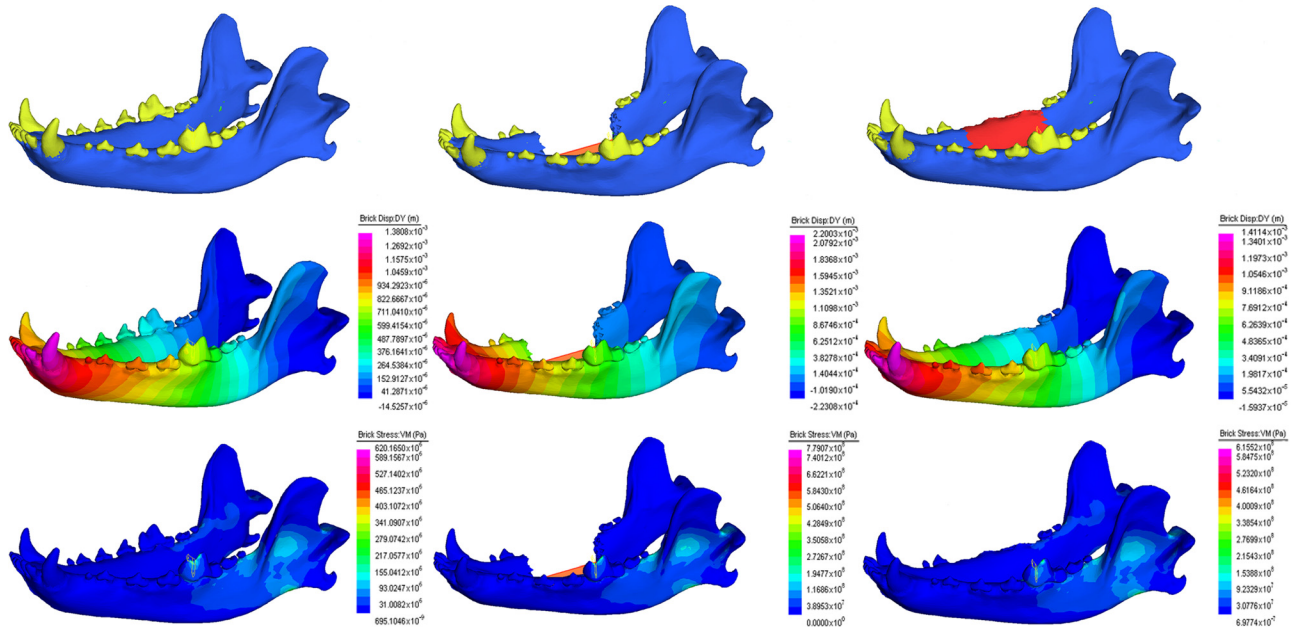
Fig. 7 Numerical results from the FEMs for the 256 N load applied at the molar position. The first column represents the model of the mandible without surgical intervention; the second column represents the mandible at the earliest bone transport stage, including the device; and the third column represents the mandible with the newly formed bone tissue 12 weeks after distraction. The first row represents the vertical deformation pattern, and the second row shows the Von Misses stress patterns.
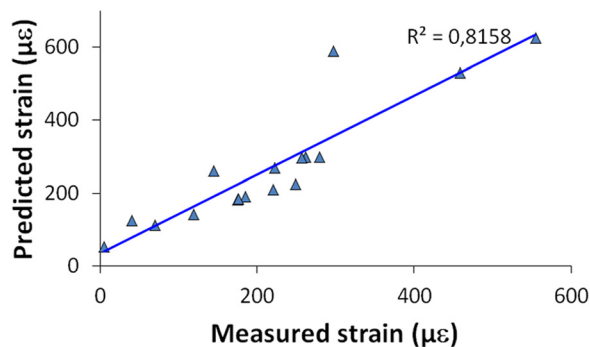

Fig. 8 Validation of the biomechanical result for BTDO using both computational and experimental results. Linear correlation between normal maximum strains recorded on the rosettes attached to the mandible and predicted maximum normal strains read from the FEMs.

symphysis were not considered as the places for distraction. In addition, the lower placement of the device is related with its double function, which provides both the active distraction and the main structural support [44].

Considering the limitations described above, the validated model supports the clinical theory that if the inflammation, pain, and infection processes are adequately controlled, the mandibular BTDO procedure could restore the mandible to a biomechanical state similar to that present prior to BTDO.

Acknowledgment

The authors are grateful to Dr. Byron W. (Pete) Benson, director and professor of Radiology at Baylor College of Dentistry, for his assistance with obtaining CT scan information for the mandible. The authors thank Gerald Hill from the animal facilities for the surgical support and tissue preparation.

This work was supported by NIH/NIDCR grants R42 DE015437-03, R43 DE017259-05, a fellowship from COLCIENCIAS-Colombia, and a fellowship from The Matsumae International Foundation (MIF)-Japan.

The author M. Elsalanty discloses to be the inventor of the *mandibular bone transport reconstruction plate*, which is covered under the patent number US7998216 B2. Dr. Elsalanty and Dr. Opperman are co-owners of Craniotech ACR Devices LLC that provided the BTRP used in testing.

Ethical approval was provided by the Texas A&M University Baylor College of Dentistry Institutional Animal Care and Use Committee.

References

[1] Codivilla, A., 1905, "On the Means of Lengthening, in the Lower Limbs, the Muscles and Tissues Which Are Shortened Through Deformity," J. Bone Joint Surg. Am., **22**(4), pp. 353–369.

[2] Abbott, L. C., 1927, "The Operative Lengthening of the Tibia and Fibula," J. Bone Joint Surg. Am., **9**(1), pp. 128–152.

[3] McCarthy, J. G., Schreiber, J., Karp, N., Thorne, C. H., and Grayson, B. H., 1992, "Lengthening the Human Mandible by Gradual Distraction," Plast. Reconstr. Surg., **89**(1), pp. 1–8.

[4] Karp, N. S., Thorne, C. H., McCarthy, J. G., and Sissons, H. A., 1990, "Bone Lengthening in the Craniofacial Skeleton," Ann. Plast. Surg., **24**(3), pp. 231–237.

[5] Ilizarov, G. A., 1989, "The Tension–Stress Effect on the Genesis and Growth of Tissues. Part I. The Influence of Stability of Fixation and Soft-Tissue Preservation," Clin. Orthop. Relat. Res., **238**, pp. 249–281.

[6] Ilizarov, G. A., 1989, "The Tension–Stress Effect on the Genesis and Growth of Tissues: Part II. The Influence of the Rate and Frequency of Distraction," Clin. Orthop. Relat. Res., **239**, pp. 263–285.

[7] Snyder, C. C., Levine, G. A., Swanson, H. M., and Browne, E. Z., Jr., 1973, "Mandibular Lengthening by Gradual Distraction: Preliminary Report," Plast. Reconstr. Surg., **51**(5), pp. 506–508.

[8] Michieli, S., and Miotti, B., 1977, "Lengthening of Mandibular Body by Gradual Surgical Orthodontic Distraction," J. Oral Surg., **35**(3), pp. 187–192.

[9] Costantino, P. D., Shybut, G., Friedman, C. D., Pelzer, H. J., Masini, M., Shindo, M. L., and Sisson, G. A., Sr., 1990, "Segmental Mandibular Regeneration by Distraction Osteogenesis. An Experimental Study," Arch. Otolaryngol. Head Neck Surg., **116**(5), pp. 535–545.

[10] Kim, S. M., Park, J. M., Myoung, H., and Lee, J. H., 2010, "Transport Disc Distraction Osteogenesis as an Alternative Protocol for Mandibular Reconstruction," J. Plast. Reconstr. Aestheth. Surg., **63**(8), pp. e644–e646.

[11] Rubio-Bueno, P., Sanroman, F., Garcia, P., Sanchez, M., Llorens, P., Nieto, S., Adrados, M., Sastre, J., De Artinano, F. O., Amde, S., Naval, L., and Diaz-Gonzalez, F. J., 2002, "Experimental Mandibular Regeneration by Distraction Osteogenesis With Submerged Devices: Preliminary Results of a Canine Model," J. Craniofac. Surg., **13**(2), pp. 224–230.

[12] Wang, J. J., Chen, J., Ping, F. Y., and Yan, F. G., 2012, "Double-Step Transport Distraction Osteogenesis in the Reconstruction of Unilateral Large Mandibular Defects After Tumour Resection Using Internal Distraction Devices," Int. J. Oral Maxillofac. Surg., 41(5), pp. 587–595.

[13] Cope, J. B., Samchukov, M. L., and Muirhead, D. E., 2002, "Distraction Osteogenesis and Histogenesis in Beagle Dogs: The Effect of Gradual Mandibular Osteodistraction on Bone and Gingiva," J. Periodontol., 73(3), pp. 271–282.

[14] Swennen, G., Schliephake, H., Dempf, R., Schierle, H., and Malevez, C., 2001, "Craniofacial Distraction Osteogenesis: A Review of the Literature. Part 1: Clinical Studies," Int. J. Oral Maxillofac. Surg., 30(2), pp. 89–103.

[15] Djasim, U. M., Wolvius, E. B., van Neck, J. W., Weinans, H., and van der Wal, K. G. H., 2007, "Recommendations for Optimal Distraction Protocols for Various Animal Models on the Basis of a Systematic Review of the Literature," Int. J. Oral Maxillofac. Surg., 36(10), pp. 877–883.

[16] Kofod, T., Cattaneo, P. M., Dalstra, M., and Melsen, B., 2005, "Three-Dimensional Finite Element Analysis of the Mandible and Temporomandibular Joint During Vertical Ramus Elongation by Distraction Osteogenesis," J. Craniofac. Surg., 16(4), pp. 586–593.

[17] Cope, J. B., Samchukov, M. L., Cherkashin, A. M., Wolford, L. M., and Franco, P., 1999, "Biomechanics of Mandibular Distractor Orientation: An Animal Model Analysis," J. Oral Maxillofac. Surg., 57(8), pp. 952–962.

[18] Cope, J. B., and Samchukov, M. L., 2000, "Regenerate Bone Formation and Remodeling during Mandibular Osteodistraction," Angle Orthod., 70(2), pp. 99–111.

[19] Lindner, D. L., Marretta, S. M., Pijanowski, G. J., Johnson, A. L., and Smith, C. W., 1995, "Measurement of Bite Force in Dogs: A Pilot Study," J. Vet. Dent., 12(2), pp. 49–52.

[20] Chopra, S., and Enepekides, D. J., 2007, "The Role of Distraction Osteogenesis in Mandibular Reconstruction," Curr. Opin. Otolaryngol. Head. Neck. Surg., 15(4), pp. 197–201.

[21] Hibbeller, R. C., 2010, Mechanics of Materials, Prentice Hall, Upper Saddle River, NJ.

[22] Castaño, M. C., Zapata, U., Pedroza, A., Jaramillo, J. D., and Roldán, S., 2002, "Creation of a Three-Dimensional Model of the Mandible and the TMJ in Vivo by Means of the Finite Element Method," Int. J. Comput. Dent., 5(2,3), pp. 87–99.

[23] Gilmore, R. S., Pollack, R. P., and Katz, J. L., 1970, "Elastic Properties of Bovine Dentine and Enamel," Arch. Oral Biol., 15(8), pp. 787–796.

[24] Jørgensen, C. S., and Kundu, T., 2002, "Measurement of Material Elastic Constants of Trabecular Bone: A Micromechanical Analytic Study Using a 1 GHz Acoustic Microscope," J. Orthop. Res., 20(1), pp. 151–158.

[25] Pressel, T., Bouguecha, A., Vogt, U., Meyer-Lindenberg, A., Behrens, B. A., Nolte, I., and Windhagen, H., 2005, "Mechanical Properties of Femoral Trabecular Bone in Dogs," Biomed. Eng. Online, 4, p. 17.

[26] Zapata, U., Opperman, L. A., Kontogiorgos, E., Elsalanty, M. E., and Dechow, P. C., 2011, "Biomechanical Characteristics of Regenerated Cortical Bone in the Canine Mandible," J. Tissue Eng. Regener. Med., 5(7), pp. 551–559.

[27] Jurvelin, J. S., Arokoski, J. P. A., Hunziker, E. B., and Helminen, H. J., 2000, "Topographical Variation of the Elastic Properties of Articular Cartilage in the Canine Knee," J. Biomech., 33(6), pp. 669–675.

[28] Scapino, R., 1981, "Morphological Investigation Into Functions of the Jaw Symphysis in Carnivorans," J. Morphol., 167(3), pp. 339–375.

[29] Boyer, R., Welsch, G., and Collings, E., 2007, Material Properies Handbook: Titanium Alloys, ASM International, Materials Park, OH.

[30] Campos, T. N., Adachi, L. K., Chorres, J. E., Campos, A. C., Muramatsu, M., and Gioso, M. A., 2006, "Holographic Interferometry Method for Assessment of Static Load Stress Distribution in Dog Mandible," Braz. Dent. J., 17(4), pp. 279–284.

[31] Kontogiorgos, E., Elsalanty, M. E., Zapata, U., Zakhary, I., Nagy, W. W., Dechow, P. C., and Opperman, L. A., 2011, "Three-Dimensional Evaluation of Mandibular Bone Regenerated by Bone Transport Distraction Osteogenesis," Calcif. Tissue Int., 89(1), pp. 43–52.

[32] Zapata, U., Halvachs, E. K., Dechow, P. C., Elsalanty, M. E., and Opperman, L. A., 2011, "Architecture and Microstructure of Cortical Bone in Reconstructed Canine Mandibles After Bone Transport Distraction Osteogenesis," Calcif. Tissue Int., 89(5), pp. 379–388.

[33] Kontogiorgos, E., Elsalanty, M. E., Zakhary, I., Nagy, W. W., Dechow, P. C., and Opperman, L. A., 2013, "Osseointegration of Dental Implants Placed Into Canine Mandibular Bone Regenerated by Bone Transport Distraction Osteogenesis," Int. J. Oral Maxillofac. Implants, 28(3), pp. 677–686.

[34] Nosaka, Y., Tsunokuma, M., Hayashi, H., and Kakudo, K., 2000, "Placement of Implants in Distraction Osteogenesis: A Pilot Study in Dogs," Int. J. Oral Maxillofac. Implants, 15(2), pp. 185–192.

[35] Trucano, T., and Post, D., 2004, "Verification and Validation in Computational Science and Engineering," Comput. Sci. Eng., 6(5), pp. 8–9.

[36] Babuska, I., and Oden, J. T., 2004, "Verification and Validation in Computational Engineering and Science: Basic Concepts," Comput. Methods Appl. Mech. Eng., 193(36–38), pp. 4057–4066.

[37] Viceconti, M., Olsen, S., Nolte, L. P., and Burton, K., 2005, "Extracting Clinically Relevant Data From Finite Element Simulations," Clin. Biomech., 20(5), pp. 451–454.

[38] Henninger, H. B., Reese, S. P., Anderson, A. E., and Weiss, J. A., 2010, "Validation of Computational Models in Biomechanics," Proc. Inst. Mech. Eng. Part H, 224(H7), pp. 801–812.

[39] Throckmorton, G. S., and Dechow, P. C., 1994, "In Vitro Strain Measurements in the Condylar Process of the Human Mandible," Arch. Oral Biol., 39(10), pp. 853–867.

[40] Panagiotopoulou, O., Curtis, N., O' Higgins, P., and Cobb, S. N., 2010, "Modelling Subcortical Bone in Finite Element Analyses: A Validation and Sensitivity Study in the Macaque Mandible," J. Biomech., 43(8), pp. 1603–1611.

[41] Marinescu, R., Daegling, D. J., and Rapoff, A. J., 2005, "Finite-Element Modeling of the Anthropoid Mandible: The Effects of Altered Boundary Conditions," Anat. Rec. A Discover. Mol. Cell Evol. Biol., 283(2), pp. 300–309.

[42] Keyak, J. H., Fourkas, M. G., Meagher, J. M., and Skinner, H. B., 1993, "Validation of an Automated Method of Three-Dimensional Finite Element Modelling of Bone," J. Biomed. Eng., 15(6), pp. 505–509.

[43] Carte, D. R., and Hayes, W. C., 1977, "The Compressive Behavior of Bone as a Two-Phase Porous Structure," J. Bone Joint Surg. Am., 59(7), pp. 954–962.

[44] Zapata, U., Elsalanty, M. E., Dechow, P. C., and Opperman, L. A., 2010, "Biomechanical Configurations of Mandibular Transport Distraction Osteogenesis Devices," Tissue Eng. Part B Rev., 16(3), pp. 273–283.